Comparisons of Boundary-Layer Transition Measurement Techniques at Supersonic Mach Numbers

R. M. Hall*
NASA Langley Research Center, Hampton, Virginia 23665
C. J. Obara†
Planning Research Corporation, Hampton, Virginia 23666
D. L. Carraway,‡ C. B. Johnson,§ R. E. Wright, Jr.,¶ and P. F. Covell**
NASA Langley Research Center, Hampton, Virginia 23665
and
M. Azzazy††
Spectron Development Laboratories, Costa Mesa, California 92626

Four different boundary-layer transition detection techniques—very thin hot films, liquid crystals, infrared imaging, and an optical interferometer—were compared using the same flat-plate model for the same tunnel conditions. The comparisons, conducted at the NASA Langley Research Center, involved not only their sensitivity to transition but also their ease of use. The thin films, as expected, gave excellent quantitative information and were used as the standard for evaluating the other techniques. Both the liquid crystals and infrared imaging were able to detect transition before the boundary-layer intermittency factor had reached 50%. The optical interferometer was unsuccessful. Conditions sampled included a range of Mach numbers from 1.5 to 2.5 and unit Reynolds numbers from 3.3 to 13.1 × 10^6/m.

Nomenclature

M = Mach number
R = Reynolds number
T = temperature, K
x = longitudinal position from leading edge of plate, m
Γ = boundary-layer intermittency factor

Subscripts
ir = location of transition as measured by infrared imaging
lc = location of transition as measured by liquid crystals
o = stagnation conditions
w = property at wall
∞ = conditions at freestream

Introduction

THE ability to experimentally determine where boundary-layer transition occurs over a test configuration is important for many reasons. For example, to compare computational drag predictions with wind-tunnel values, it is necessary to know where transition actually occurred on the wind-tunnel model. Also, for high angle-of-attack research, knowing the state of the boundary layer on the forebody of a configuration will help determine whether or not the data will have to be corrected before being applicable to full-scale flight.

Received May 15, 1989; presented as Paper 89-2205 at the AIAA 7th Applied Aerodynamics Conference, Seattle, WA, July 31–Aug. 2, 1989; revision received March 20, 1990; accepted for publication June 11, 1990.

*Senior Research Engineer. Associate Fellow AIAA.
†Senior Aerodynamics Engineer; currently Research Engineer, NASA Langley Research Center, Hampton, VA 23665.
‡Research Engineer. Member AIAA.
§Senior Research Engineer. Member AIAA.
¶Instrumentation Engineer.
**Research Engineer. Senior Member AIAA.
††Research Scientist. Member AIAA.

The present effort was initiated at the NASA Langley Research Center to compare four different techniques that had been previously used[1-4] to measure transition under widely varying wind-tunnel and flight conditions. The four test techniques were very thin hot films in a constant temperature mode, liquid crystals in a shear sensitive mode, passive infrared imaging, and an optical interferometer. The present objective was to use all four techniques to measure transition over the same model for the same conditions. The four techniques were to be judged by their sensitivity to transition as well as their ease of use. An additional objective was to determine whether the qualitative techniques—liquid crystals and the infrared imaging—were responding to boundary-layer transition at the beginning, in the middle, or at the end of the transition process.

Experimental Apparatus

Unitary Plan Wind Tunnel

The Unitary Plan Wind Tunnel[5] (UPWT) is a closed-circuit pressure tunnel with two 1.2 × 1.2 × 2.1-m test sections. Test section no. 1, which was used during the investigation, can provide a range of freestream Mach number M_∞ from 1.46 to 2.86. The actual values of M_∞ used for the experiment were 1.5, 2.0, and 2.5 The total pressure of the tunnel was varied during the current test to provide a range of unit Reynolds number R/m from 3.3 to 13.1 × 10^6 (or R/ft from 1.0 to 4.0 × 10^6). The tunnel has the capability of varying its total temperature T_o, although for the present experiment it was kept at a value of 325 K.

Flat-Plate Model

The model used for the present tests[6] had a spatula-shaped flat upper surface on which there was a removable cavity plate that could be modified or changed during the course of the experiment; see Fig. 1. The model was constructed with a model support housing on its bottom side, as seen in Fig. 2. This bottom support housing begins with a slightly blunted 20-deg half-angle conical fairing. This fairing posed a complication for the present experiment because the local adiabatic wall temperature for this fairing was higher than the local adiabatic

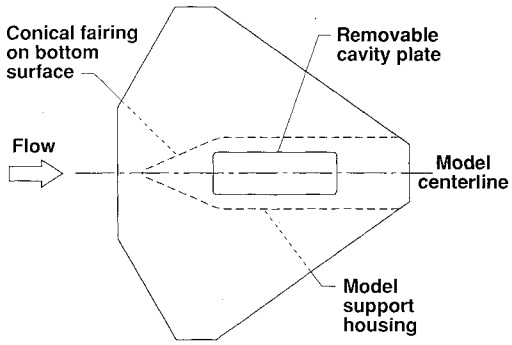

Fig. 1 Schematic of flat-plate model showing removable cavity plate and location of support structure on bottom surface.

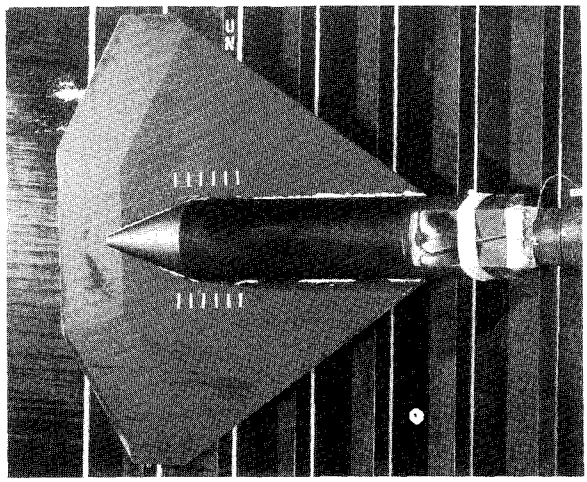

Fig. 2 Photograph showing bottom of plate. Note conical fairing in front of model support housing.

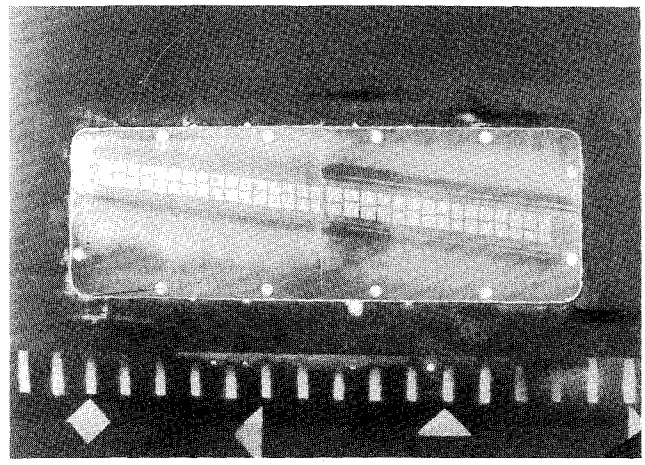

Fig. 3 Stainless-steel cavity plate with thin films installed.

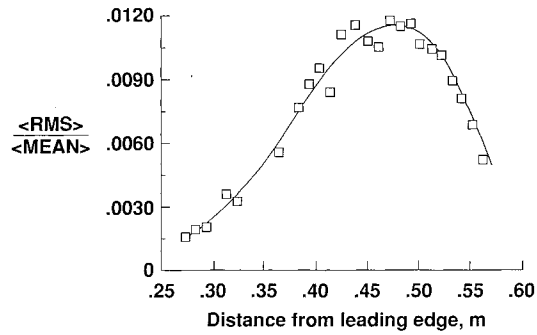

Fig. 4 Averages of signal rms divided by averages of signal mean for thin films. $M_\infty = 1.5$, $R/m = 9.8 \times 10^6$.

wall temperature for the flat-plate surface on the top of the model. Consequently, heat was conducted from the fairing to the upper measurement surface and could have triggered premature boundary-layer transition. Fortunately, as will be discussed later, the impact of the heat conduction on transition location is expected to be insignificant.

There was also one configuration difference between the tests with the liquid crystals and the thin films and the tests using infrared imaging. That difference was the use of a stainless-steel cavity plate for the liquid crystals and the thin films and the use of a Bakelite (an insulator) cavity plate for the infrared measurements. This configuration change to Bakelite was made to reduce the heat conduction from the lower fairing, which was resulting in larger temperature differences than the temperature differences due to transition from laminar to turbulent flow.

Transition Detection Techniques

Thin Films

The constant-temperature thin films used for this study were vapor-deposited on a stainless-steel cavity plate; see Fig. 3. The 31 hot-film sensors consisted of a pattern of nickel film (about 0.2 μm thick) that was vapor deposited on a dielectric substrate consisting of parylene C and fused silica (about 8.9 μm thick). The electrical connectors for the driving electronics were vapor-deposited aluminum leads (about 0.5 μm thick). These surface-deposited electrical leads connected the nickel-film and model-surface electrical connectors. The entire system—films, substrate, and aluminum leads—had a total roughness height of less than 10.2 μm. A more complete description of the films is contained in Ref. 1. During the present experiment, operational gauges extended from 0.28 to 0.57 m from the leading edge of the flat plate.

The row of thin films gave information concerning transition along the line of gauges. An example of the type of thin film data, reduced on-line, is shown in Fig. 4. Two averages were calculated for each film—the average of the root-mean-square (rms) of the voltage fluctuations and an average of signal mean voltage. These averages were the result of four different 1-s measurements made at approximately 30-s intervals—all the gauges were sampled sequentially, each for 1-s, and then the cycle was repeated for three additional times. A ratio of these averaged quantities, ⟨rms⟩/⟨mean⟩, indicative of local turbulence level, was then plotted as a function of distance from the leading edge of the flat plate (the cavity plate begins at a distance 0.24 m from the leading edge of the model). As seen in the figure, the activity at the gauges varied in a relatively continuous fashion over the cavity plate.

The shape of this plot is very similar to the shapes recorded by Owen.[7] As discussed by Owen, the hump, or peak, in the midsection of the curve indicates the boundary-layer transition region. The peak is a result of voltage fluctuations caused by the passage of turbulent spots[8] as well as an increase in overall voltage fluctuation level due to the change in the flow from laminar to turbulent. Laminar flow, if present, is found on the plot upstream of the peak region where the ⟨rms⟩/⟨mean⟩ values are low and where the curve has little or no slope. Fully turbulent flow, if present, is found downstream of the peak region where the ⟨rms⟩/⟨mean⟩ values are moderate and where the curve again has little or no slope.

The modest scatter in the data for the natural transition region was due to the movement of the transition region over the plate (as evidenced earlier by the liquid crystals). Since the thin films were sampled sequentially, not simultaneously, the effective location of the transition region could be different from sample period to sample period. Subsequent tests, not presented here, where transition was fixed on the same plate,

exhibited no scatter—verifying that the scatter illustrated in Fig. 4 was indeed due to the movement of natural transition and not because of sensitivity differences in the films.

Visual analysis of the individual signal traces from the thin films found that the location where the intermittency factor Γ was 0.5—that is, where the boundary-layer state was turbulent half of the time and laminar half of the time—corresponded approximately to the location of the maximum in the plot of $\langle rms \rangle / \langle mean \rangle$. For the conditions of Fig. 4, $M_\infty = 1.5$ and $R/m = 9.8 \times 10^6$, $\Gamma = 0.5$ occurred at a station approximately 0.50 m from the leading edge.

As mentioned by Owen,[7] the location where Γ becomes 0.5 is one of three useful and easily measured locations characterizing the transition process. The other two locations are where the onset of turbulence fluctuations begin ($\Gamma \simeq 0.0$) and where the flow becomes fully turbulent ($\Gamma = 1.0$).

Liquid Crystals

Liquid crystals have properties of both liquid-phase and solid-phase materials. Although appearing fluid-like, liquid crystals exhibit optical properties of solid crystals. As illustrated in Fig. 5, liquid crystals scatter incident light if that light corresponds in wavelength to a characteristic pitch length p of the crystals. Fortunately, the helix pitch lengths are in the range of visible light. This pitch length can be altered by temperature and shear stress. Thus, liquid crystals selectively reflect discrete wavelengths (color) of light in response to differences in temperature or shear stress. Since the fundamental chemical structure is unaffected by these differences, a liquid crystal coating can respond rapidly to changes in temperature and shear stress.

For the present test, the liquid crystals were employed in a shear-sensitive mode. That is, the crystals were prepared so that the temperature range at which their color changed was above the temperatures seen in the experiment. Consequently, the crystals were only responding to differences in the applied shear stress and had sufficient frequency response to reflect tunnel unsteadiness in turbulent wedges initiated by model defects or sand grit. As discussed in Ref. 9 for a flight test using the liquid crystals, the time response of the liquid-crystal coating was on the order of a fraction of a second; see both Refs. 2 and 9 for more technical details and for examples of liquid crystal technology applied to flight research.

The application of the liquid-crystal transition visualization technique requires care in the preparation of the test surface. It is important that the surface be painted with a deep-matte, flat-black paint that is resistant to the solvents used to thin the liquid crystals. This deep-matte texture provides a surface to which a very thin liquid crystal coating can best adhere, while the black paint allows for reflection of all wavelengths of visible light. Another important factor is the arrangement of adequate lighting to provide clear visual data. Improperly placed lights and cameras can produce glaring highlights that can diminish the worth of the experiment. The scattered light also depends on viewing angle; consequently, for the present test, the photographic equipment was always aligned normal to the model surface.

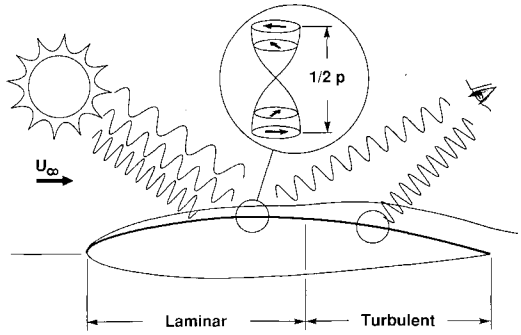

Fig. 5 Schematic illustrating selective scattering of light by liquid crystals.

The liquid crystals were relatively simple to use during the experimental program. The solution was sprayed onto the model surface and then smoothed, or aligned, by stroking a spongelike tool in the flow direction over the liquid crystal coating. The crystals then would remain on the model until 'scrubbed'' off by the aerodynamic shear stresses during tunnel operation. The period of useful testing depended on the tunnel dynamic pressure. If the tunnel was being operated at low values of unit Reynolds number (low dynamic pressure), the crystals could be utilized for up to 60 min. If the tunnel was being operated at the upper range of unit Reynolds number (high dynamic pressure), the useful lifetime of the liquid crystals was typically 30 min.

Examples of the liquid crystal information at $M_\infty = 1.5$ for both artificially tripped turbulent wedges as well as for natural transition are shown in Fig. 6. In the left photograph, the liquid crystals highlight four turbulent wedges that resulted from defects in the model surface. As seen, the turbulent wedges, with their high values of shear stress, appear to have a light green color whereas the laminar flow region, with its lower values of shear stress, appears to have a brownish red color. At this value of $Re/m = 3.3 \times 10^6$, the flow over the model would have been entirely laminar were it not for the added sand grit and the microphones embedded in the surface (not part of the present test). The glare regions on the top and bottom sections of the flat plate resulted from the lighting used to illuminate the crystals. The measurement area of interest was in the middle of the model.

The right photograph in Fig. 6 illustrates an example of detecting natural transition at a higher value of unit Reynolds number, $Re/m = 9.8 \times 10^6$. For this example, the sharp gradients in color seen across the edges of the turbulent wedges are not present for natural transition because of the length over which the transition process takes place, as was seen in

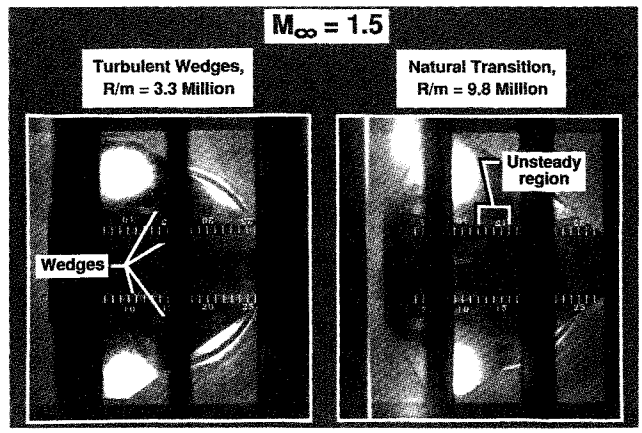

Fig. 6 Examples of liquid crystal information.

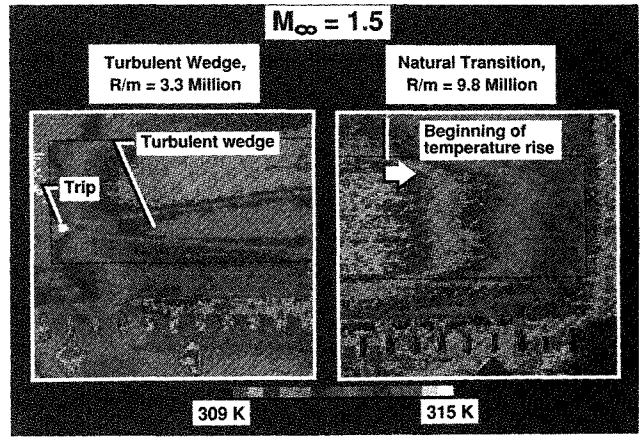

Fig. 7 Examples of infrared imaging.

Fig. 4. Nevertheless, the central region of the flat plate is clearly the brownish red color in front of the longitudinal region labeled "unsteady region" in the figure. Aft of the unsteady region, the color has turned greenish, indicative of turbulent flow with its higher value of shear stress. During real-time viewing, or on review of the video tape, the unsteady region fluctuated in color between the brownish red and the greener colors. This fluctuation was attributed to the apparent movement in the position of natural transition. For purposes of this study, the liquid crystals were said to have detected the onset of transition at the upstream end of the unsteady region.

A significant advantage of this technique was that it permits visualization of the entire surface over which it is applied. In other words, at one instant of time, a two-dimensional picture of the laminar and turbulent regions over the flat plate could be seen and recorded.

Infrared Imaging

An infrared imaging technique was employed to determine boundary-layer transition by measuring differences in wall temperature that result from changes in the recovery factor as the flow transitions from laminar to turbulent. These differences are a function of many things including the flow state and the thermal conductance within the model. The imager used rotating mirrors for the scanning system, had a temperature sensitivity of 0.1 K, an 8–12 μm passband, and was cooled with liquid nitrogen. A zinc selenide window was used to permit optimal signal transmission.

In most previous experiments to detect natural transition with infrared imagers, a low thermal conductance model skin was used to eliminate thermal conductance from within the model. The original objective of the present test was to attempt to use a stainless-steel plate (painted black) because of the use of stainless steel as the material on which the very thin films were mounted. It was hoped that significant temperature transients could be introduced into the tunnel circuit in order to highlight natural transition, as had been employed by Crowder in low speed and transonic testing.[10]

Although the strong temperature gradients associated with the turbulent wedge were visible on the stainless-steel plate, the weak temperature gradients associated with natural transition were not apparent because of lateral heat conduction within the plate. This lateral heating resulted from conduction within the metal model of the heat being generated by the conical fairing on the bottom surface. Introducing temperature transients into the tunnel circuit took longer than the time it took for the heat conduction within the model to readjust to the change and, consequently, did not highlight natural transition. As a result, an unpainted Bakelite plate was fabricated to the identical dimensions of the original stainless-steel plate and was used for the data reported herein.

The comparable infrared images for the same two examples illustrated in Fig. 6 are shown in Fig. 7. In the left photograph, the heating resulting from a turbulent wedge is clearly seen by the red and orange colors representing the higher temperatures. (The temperature scale was calculated for the emissivity of the Bakelite plate, which is outlined by the dotted black lines, and only applies to the colors within the dotted line because the emissivity of the painted stainless steel was different. The hot region in front of the Bakelite plate is due to the heating from the conical fairing.) The example of natural transition is shown in the right photograph, which shows the gradual heating of the plate as the colors change from the blues through the greens and up to the reds and oranges. The heating is, of course, indicative of the transition process. For the present experiment, onset of transition was taken to be the position where the cavity plate wall temperature began to increase along the plate.

Optical Interferometer

The boundary-layer transition detector, developed by Spectron Development Laboratories,[4] used a differential interferometer to nonintrusively measure the frequency of density fluctuations in the compressible boundary layer as a means of assessing whether the boundary layer was laminar, transitioning, or turbulent. The heart of the device was a highly sensitive differential interferometer capable of detecting optical pathlength differences on the order of one-thousandth of the wavelength of the laser light. The sensitivity of the interferometer was due, in part, to a compensator loop. This loop adjusted the phase relationship between the two beams of the interferometer to optimize the performance of the interferometer and to null out any low-frequency (less than 10 kHz) noise. Twin photodetectors generated the output voltage signal as well as the information for controlling the compensator loop. Electronic signal processing was also essential for real-time assessments of the boundary-layer activity.

Although this interferometer was successful in measuring transition in an atmospheric, transonic wind tunnel as reported in Ref. 4, no useful data were obtained in the present test. The apparent reason for the failure was that the signal to noise ratio was three times lower in the present test than it was in the transonic test.

Results and Discussion

Data were taken for each of the four different techniques for the same model configuration, with the exception of the cavity plate material, and at the same conditions. Three values of M_∞—1.5, 2.0, and 2.5—were examined for values of R/m between 3.3×10^6 and 13.1×10^6.

The criteria for determining onset was different for all three of the successful techniques and will be summarized as follows. For the thin film technique, onset is described by the three distinctive locations that can be characterized by thin films—$\Gamma \simeq 0.0$, $\Gamma = 0.5$, and $\Gamma = 1.0$. As mentioned, the thin films only extended from 0.28 to 0.57 m downstream of the leading edge of the flat plate. For the liquid crystals, the onset of transition was taken to be the beginning of the unsteady, fluctuating region between the color associated with the laminar and the color associated with the turbulent region. For the infrared imaging, onset was taken to be the location at which the camera detected an increase in T_w. The respective uncertainties in the measurements of onset by the liquid crystals and the infrared imaging are ± 0.05 and ± 0.03 m. The uncertainty in the Γ locations determined by the thin films is also ± 0.03 m.

The data comparisons will be presented in two formats. The first series of comparisons will illustrate, for each Mach number tested, comparisons of the thin film output, the liquid crystal onset points, and the infrared onset points. These comparisons will be for $R/m = 9.8 \times 10^6$. The second series of comparisons will summarize as a function of R/m onset locations for $\Gamma \simeq 0.0$, $\Gamma = 0.5$, $\Gamma = 1.0$, the liquid crystals and the infrared imaging.

Comparison of Onset for $R/m = 9.8 \times 10^6$

The first series of comparisons are presented in Figs. 8a–8c. For the $M_\infty = 1.5$ data, Figs. 8a, the liquid crystal technique detected onset at $x = 0.30$ m, which is very close to the location where the thin film gauges detected the beginning of turbulent activity. On the other hand, the infrared measurements detected onset of activity at $x = 0.40$ m, which is about midway between the $\Gamma \simeq 0.0$ and $\Gamma = 0.5$ locations. At this lowest value of M_∞, the relative performance of the liquid crystals is superior to the infrared system.

The second comparison is shown in Fig. 8b for $M_\infty = 2.0$. For this case, the onset according to liquid crystals appeared midway between the $\Gamma \simeq 0.0$ and $\Gamma = 0.5$ locations. Conversely, the infrared onset occurred earlier. Note that the width of the normalized rms peak is growing smaller and the magnitude of the peak level is decreasing. For this value of M_∞, fully turbulent flow, the $\Gamma = 1.0$ location, occurred at $x = 0.52$ m.

The comparison at a value of $M_\infty = 2.5$, Fig. 8c, continues the trend that the magnitude as well as the width of the peak continues to decrease with increasing M_∞. In this case, the liquid crystals detected transition at $x = 0.25$ m and the infrared technique detected transition at $x = 0.26$ m. The location of $\Gamma \simeq 0.0$ was upstream of the first operational gauge location, which was at 0.27 m. It is important to note that both the liquid crystal and the infrared techniques flagged transition close to what appears to be the beginning of the peak in the thin-film plot.

Comparison of Onsets for All Values of R/m

Figures 9a–9c summarize the performance of the techniques over the range of R/m tested for each of the three values of M_∞ examined. For the $M_\infty = 1.5$ data, Fig. 9a illustrates that the liquid crystals changed their color at distances closer to the location of $\Gamma \simeq 0.0$ than of $\Gamma = 0.5$. In terms of distance, the liquid crystals detected onset at least 0.13 m in front of the $\Gamma = 0.5$ location. In contrast, the infrared imaging was not quite as sensitive to transition and generally detected it about 0.08 or 0.10 m upstream of the $\Gamma = 0.5$ location. The sensitivity of both the liquid crystals and the infrared imaging appeared to be independent of R/m and both sets of data appear to follow parallel trends.

For the $M_\infty = 2.0$ data, Fig. 9b shows that, again, both the liquid crystals and the infrared instrumentation registered effects of transition before the $\Gamma = 0.5$ location. In this case, both the liquid crystals and the infrared imaging generally detected transition between 0.05 and 0.08 m upstream of the 0.5 location. In fact, only one line is drawn in Fig. 9b to represent both the trends of the liquid crystals and the infrared imaging. At this higher value of M_∞, the infrared imaging is performing comparably to the liquid crystals.

Finally, Fig. 9c shows the data for $M_\infty = 2.5$. With the exception of the $R/m = 3.3 \times 10^6$ data, the liquid crystals and the infrared are performing equally well and both techniques appear to detect transition very close to the onset of turbulent activity in the boundary layer, where $\Gamma \simeq 0.0$. At $R/m = 3.3 \times 10^6$, both techniques seem to lack the sensitivity that they appear to have for values of $R/m \geq 6.6 \times 10^6$. It is unclear why there appears to be a R/m sensitivity at this value of M_∞.

Another way to compare onset as measured by the three different techniques is to summarize the Reynolds number at transition. These data are compared in Table 1. As seen in the table, the Reynolds number corresponding to the location of transition detection varies from technique to technique. Of course, the region of transition is itself quite broad, as highlighted by the thin film data in Table 1 as well as by Fig. 9.

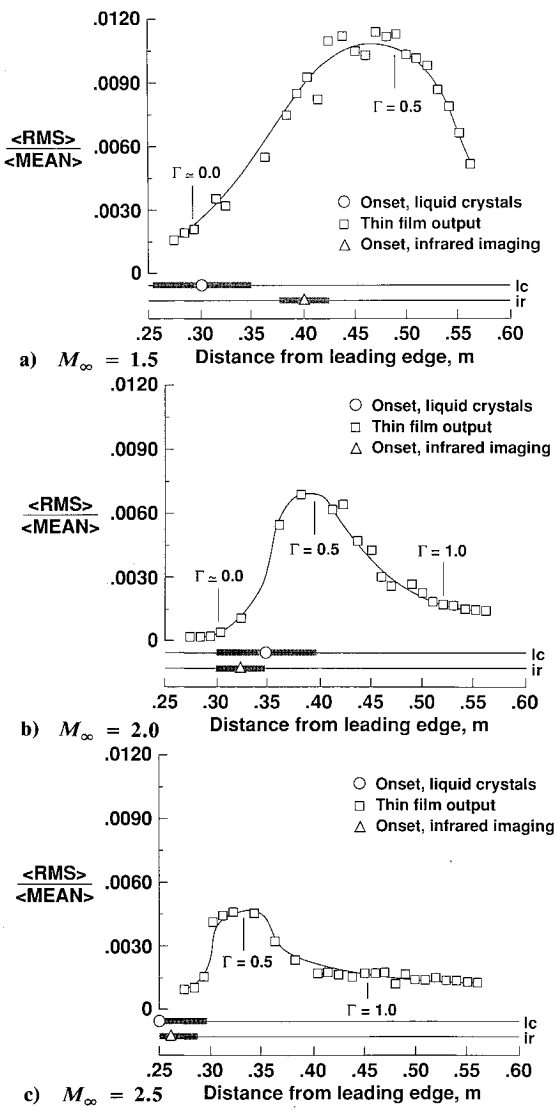

Fig. 8 Comparison of thin film voltages to onset determined by other techniques. $R/m = 9.8 \times 10^6$.

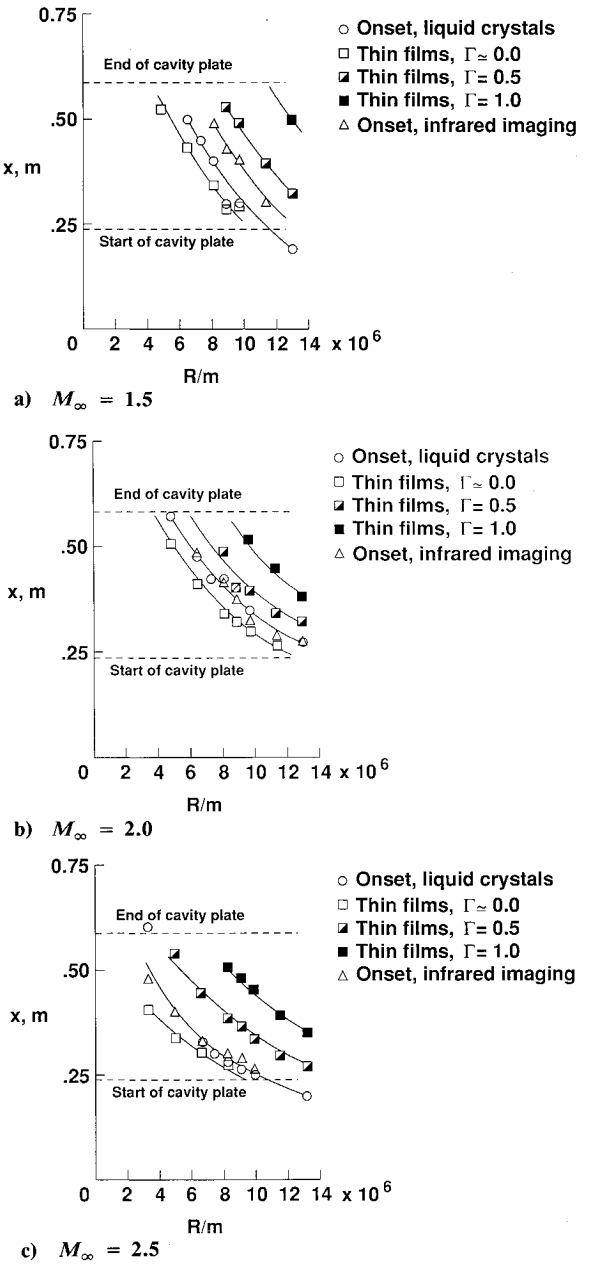

Fig. 9 Comparison summary of techniques.

Table 1 Reynolds numbers ($\times 10^6$) at given locations

M_∞	R/m	R_{lc}	R_{ir}	$R_{\Gamma=0}$	$R_{\Gamma=0.5}$	$R_{\Gamma=1.0}$
1.5	3.3	——[a]	——	——	——	——
1.5	4.9	n/a[b]	——	2.6	——	——
1.5	6.6	3.3	——	2.9	——	——
1.5	7.4	3.4	n/a	n/a	n/a	n/a
1.5	8.2	3.3	4.1	2.9	——	——
1.5	9.0	2.8	3.9	2.6	4.8	——
1.5	9.8	3.0	4.0	2.9	4.9	——
1.5	11.5	n/a	3.5	——	4.6	——
1.5	13.1	2.5	——	——	4.3	6.7
2.0	3.3	——	——	——	——	——
2.0	4.9	2.9	——	2.6	——	——
2.0	6.6	3.2	3.3	2.8	——	——
2.0	7.4	3.2	n/a	n/a	n/a	n/a
2.0	8.2	3.5	3.4	2.9	4.1	——
2.0	9.0	3.7	3.4	3.0	3.6	——
2.0	9.8	3.5	3.3	3.0	4.0	5.2
2.0	11.5	n/a	3.4	3.1	4.0	5.2
2.0	13.1	3.7	3.7	——	4.3	5.1
2.5	3.3	2.0	1.6	1.4	——	——
2.5	4.9	n/a	2.0	1.7	2.7	——
2.5	6.6	2.2	2.2	2.0	3.0	——
2.5	7.4	2.3	n/a	n/a	n/a	n/a
2.5	8.2	2.4	2.5	2.3	3.2	4.2
2.5	9.0	2.4	2.6	——	3.3	4.4
2.5	9.8	2.5	2.6	——	3.3	4.5
2.5	11.5	n/a	——	——	3.5	4.6
2.5	13.1	2.7	n/a	——	3.6	4.7

[a]Data outside of instrumentation range. [b]Not available.

Nonadiabatic Effects

As mentioned, there was a concern during the experiment that the heat conducted from the conical fairing on the lower model support structure to the top surface would lead to reduced transition Reynolds numbers. To estimate this impact on the transition Reynolds numbers, available infrared measurements were used to determine how much the temperature of the flat plate was in excess of its adiabatic temperature. These infrared measurements revealed values of excess temperature on the order of 2.8 K. Using this value of excess wall temperature, data by Dougherty and Fisher[11] suggest that the reduction in transition Reynolds number would be 7%, based on flight data from a 10-deg cone.

This estimate of 7% reduction in transition Reynolds number may, however, be too high due to an observation by Czarnecki and Sinclair[12] that the impact of heating on transition will be reduced if there are disturbances already in the flow that result in relatively low transition Reynolds numbers. A comparison of transition Reynolds numbers by Fisher and Dougherty[13] between the 10-deg cone in flight and the same cone in the UPWT indicated transition Reynolds numbers in flight about 2.5 times higher than in the UPWT at values of $M_\infty = 1.6$ and 2.0. These findings, as well as noise measurements by Harvey,[14] establish that the disturbance level in UPWT is higher than in the cone flight data. Consequently, the observation by Czarnecki and Sinclair[12] would suggest that the reduction in transition Reynolds number due to heating during the current test will be less than the 7%. Consequently, any impact of the nonadiabatic heating with or without the Bakelite plate will be insignificant, given the experimental uncertainties in the present experiment.

Comparative Ease of Use and Utility

The techniques used varied greatly in their capabilities as well as in their ease of use. The very thin hot films required a rather large amount of supporting instrumentation and experience[1] to do the present type of measurements. In this sense, using thin films required a complicated setup and experienced personnel. Also, applying the hot films to the metal cavity plates for the present experiment was a challenge that required specialists skilled in microelectronic fabrication techniques. On the other hand, results from this approach are quantitative in nature and reliable. This technique served as the yardstick with which to measure the other techniques.

During the present test the simplest technique to employ was the liquid crystals. The crystals were simply sprayed onto the model, which had been painted black. Data acquisition took only as long as it took to take a picture or to record on video tape. A picture so taken contained data for the entire surface at one time. Some expertise and judgment are necessary to choose and mix the liquid crystals. Picking a color whose contrast is clear in the tunnel as well as choosing a temperature reaction range outside those temperatures found during the experiment are both important. Rapid response of the liquid crystal coating was observed during the test. The fluctuations in the tunnel turbulence were observed by the liquid crystals as fluctuations in the turbulent wedges generated on the model.

The infrared imaging approach was again a relatively simple installation. Its exciting potential is that the model does not, in contrast to the liquid crystal technique, have to be accessed during the test. Thus, data acquisition can be continuous and uninterrupted as long as the tunnel operates. As advocated by Quast,[15] and confirmed during the present study, an insulating coating should be applied to a metal model to reduce the internal heat conduction that can mask the adiabatic wall temperature differences resulting from natural transition.

Conclusions

The present experimental program compared four different techniques that had previously been used to measure boundary-layer transition under widely varying conditions. This comparison was done by applying all four techniques to the same model at the same conditions. Three of these techniques—thin films, liquid crystals, and infrared imaging—worked well while the fourth technique—an optical interferometer—did not. The thin films, while having the most complicated installation and requiring the most support instrumentation, provided the most reliable and quantitative indicator of the details of the transition process. The liquid crystals and the infrared imaging both gave indications of boundary-layer transition before the intermittency factor reached 0.5, as measured by the thin films.

References

[1]Johnson, C. B., Carraway, D. L., Hopson, P., Jr., and Tran, S. Q., "Status of a Specialized Boundary-Layer Transition Detection System for Use in the U.S. National Transonic Facility," *Proceedings of the ICIASF Record,* Williamsburg, VA, June 22-25, 1987, Institute of Electrical and Electronics Engineers, New York, pp. 141-155.

[2]Gall, P. D., and Holmes, B. J., "Liquid Crystals for High-Altitude In-Flight Boundary-Layer Flow Visualization," AIAA Paper 86-2592, Sept.-Oct. 1986.

[3]Brandon, J. M., Manuel, G. S., Wright, R. E., and Holmes, B. J., "In-Flight Flow Visualization Using Infrared Imaging," AIAA Paper 88-2111, May 1988.

[4]Azzazy, M., Modarress, D., and Hall, R., "Optical Boundary-Layer Transition Detection in a Transonic Wind Tunnel," *AIAA Journal,* Vol. 27, No. 4, April 1989, pp. 405-410.

[5]Jackson, C. M., Jr., Corlett, W. A., and Monta, W. J., "Description and Calibration of the Langley Unitary Plan Wind Tunnel," NASA TP-1905, Nov. 1981.

[6]Wilcox, F. J., Jr., "Drag Measurements of Blunt Stores Tangentially Mounted on a Flat Plate at Supersonic Speeds," NASA TP-2742, Sept. 1987.

[7]Owen, F. K., "Transition Experiments on a Flat Plate at Subsonic and Supersonic Speeds," *AIAA Journal,* Vol. 8, No. 3, 1970, pp. 518-523.

[8]Emmons, H. W., "The Laminar-Turbulent Transition in a Boundary Layer," *Journal of the Aeronautical Sciences,* Vol. 18, No. 7, 1951, pp. 490-498.

[9]Holmes, B. J., and Obara, C. J., "Advances in Flow Visualization Using Liquid Crystal Coatings," Society of Automotive Engineers, TP 871017, April 1987.

[10]Crowder, J. P., "Recent Advances in Flow Visualization at Boeing Commercial Airplanes," 5th International Symposium on Flow Visualization, Prague, Czechoslovakia, Aug. 1989.

[11]Dougherty, N. S., Jr., and Fisher, D. F., "Boundary-Layer Transition on a 10-Degree Cone: Wind Tunnel/Flight Data Correlation," AIAA Paper 80-0154, Jan. 1980.

[12]Czarnecki, K. R., and Sinclair, A. R., "An Investigation of the Effects of Heat Transfer on Boundary-Layer Transition on a Parabolic Body of Revolution (NACA RM-10) at a Mach Number of 1.61," NACA Rept. 1240, 1955.

[13]Fisher, D. F., and Dougherty, N. S., Jr., "Flight and Wind-Tunnel Correlation of Boundary-Layer Transition on the AEDC Transition Cone," AGARD Flight Mechanics Panel Symposium, Cesme, Turkey, Oct. 11–14, 1982.

[14]Harvey, W. D., "Some Anomalies Between Wind-Tunnel and Flight Transition Results," AIAA Paper 81-1225, June 1981.

[15]Quast, A., "Detection of Transition by Infrared Image Technique," *Proceedings of the ICIASF Record,* Williamsburg, VA, June 22–25, Institute of Electrical and Electronics Engineers, New York, 1987, pp. 125–134.

Color reproductions courtesy of NASA Langley Research Center